Aerofoils For Morphing Wings

Joshua Rajendran (4S208)
Qian Runshi (4S320)

Hwa Chong Institution (High School)

A. Abstract

Airfoils in Unmanned Air Vehicles (UAVs) have flaps and slats for control surfaces on them, which creates surface discontinuities and disrupts airflow, hence harming aerodynamic efficiency. While current solutions exist, such as using fibreglass instead of aluminium in an UAV and installing sharklets on the airfoils, these all have some significant drawbacks, such as a resin that weakens and rolling due . We decided to design morphing wings that can change its geometric shape during flight and hence negate the need for these surfaces, improving aerodynamic efficiency. We then modeled several airfoils with varying ratios of the leading edge and trailing edge using Autodesk Fusion 360 based on the NACA 0012 airfoil, and then we tested them using Computational Fluid Dynamics (CFD) software at two wind speeds. Our results indicated that the optimal ratio for an airfoil is 2:2, which improved aerodynamic efficiency by an average of 14.5%. We concluded that morphing wings are suitable for use in UAVs because they increase aerodynamic efficiency by an average of 9.05%. By using morphing wings in UAVs, their mobility and efficiency can be increased, allowing for better drones and greener travel which is more beneficial for the environment due to reduced fuel

emissions. However, some limitations are the lack of wind tunnel testing which can complement our data to provide more realistic results. Furthermore, the aerofoil we used is not ideal for comparing to UAVs, and hence some recommendations include analysis of aerofoils used in current UAVs.

B. Introduction

Unmanned air vehicles are becoming an increasingly important technology in military and commercial applications. UAVs such as General Atomics Aeronautical Systems (GA-ASI)'s MQ-9B Sky Guardian functions as a multi-faceted drone. It is capable of maritime surveillance, human and disaster assistance and pollution detection **(AIN Online, 2017).** Hence, there is a clear need for drones in the modern world.

Conventional UAVs consist of a propulsion system, a lifting system and control systems. In the aerofoils of common UAVs, flaps are attached to the trailing edge of the wing as a means to control the UAV. The presence of these flaps creates camber change and can alter the lift coefficient of the aircraft. As a result, flaps are paramount in instances such as takeoff to allow aircraft to ascend quickly **(Boldmethod, 2015).**

However, there lies a problem as these flaps create surface discontinuities on the wings, causing complex airflow, thus harming aerodynamic efficiency. This is a major problem as it unnecessarily decreases lift and increases drag. Hence, there is a need for morphing wings. Morphing wings are wings that are able to change their geometric shape during flight, and replace flaps as well as ensuring smooth airflow. This can benefit both fuel and aerodynamic efficiency by reducing unnecessary drag caused by rigid control surfaces such as flaps **(Aviation Voice, 2016).**

Current solutions to improve the aerodynamic efficiency of UAVs include Airbus's sharklets technology and the use of composite materials. Fibreglass is used in place of aluminium in some parts of aircraft, as it is around 7% lighter, and more versatile. However, composite materials are more costly than aluminium, harder to repair and is risky to use as the resin in fibreglass can weaken at temperatures as low as 150°C **(Thyssenkrupp Aerospace, 2018)**. Another solution is sharklets on aircraft. They reduce the effect of vortex drag. It redirects the air and reduces the size of wingtip vortices, reducing drag and increasing fuel efficiency by up to 3.5%. However, when there is external turbulence, the sharklets will cause the aircraft to roll a little more than normal **(The Engineer, 2017).**

Hence, there is an apparent need for morphing wings to increase the aerodynamic efficiency of UAVs to a greater extent, allowing for greener travel, reducing fuel emissions. With greater efficiency, morphing wings would also facilitate the military scene by allowing militaries to integrate a faster and better drone into their systems. Morphing wings also enable UAVs to make sharper turns and have better omni-directional mobility by allowing users to change the extent of actuation of wing.

Hence, this project aims to design morphing wing aerofoils and investigate the extent to which morphing wings improve aerodynamic efficiency, and the optimal actuation of varying rigid:flexible lengths of the aerofoil for Unmanned Air Vehicles (UAVs). This is done by testing the aerodynamic efficiency of the NACA 0012 airfoil, a symmetrical airfoil, using Computational Fluid Dynamics (CFD). CFD is used because it allows for collection of many different types of data sets, such as pressure, velocity, temperature across a body, providing a realistic simulation. We also decided to test two speeds of airflow, at 13m/s and 20m/s to obtain results for low speed and high speed UAVs.

C. Solution Design

Equation of Aerofoil:

$$y_t = 5t\,\left[0.2969\sqrt{x} - 0.1260x - 0.3516x^2 + 0.2843x^3 - 0.1015x^4\right]$$

- ***x*** is the position along the chord from 0 to 1.00, (0 to 100%)
- **y.*t*** is the half thickness at a given value of *x* (centerline to surface), and
- ***t*** is the maximum thickness as a fraction of the chord (so *t* gives the last two digits in the NACA 4-digit denomination divided by 100)

This equation was derived for the NACA aerofoils by NACA in 1932. **(Jacobs., Ward. & Pinkerton., 1932)**

Control Airfoil Design:

The stock NACA 0012 airfoil was generated in Autodesk Fusion 360 using the inbuilt airfoil generator tool. The half-cosine spacing option was selected so that the curve was smooth. 120 points per side were used to model this airfoil. The airfoil was extruded to 1⁄3 cm and then scaled by a factor of 12 so that the length became 12 cm while the width became 4 cm. A block was created touching the tip of the airfoil. From this block, a plane was extruded to a predetermined length dependent on the ratio of the airfoil being created. This plane was used to split the airfoil body. The newly split portion was then rotated about the split axis to an angle of 16.19^{o}, an angle held consistent across all the control and experimental groups. The bodies were then recombined with the two airfoils now joined by a 6 mm x 3 mm piece.

Figure 1.1: Control Airfoil with ratio 6:2. Notice how the rigid edge and flexible edge are separated by a small box connecting them together so as to mimic the real-life airfoil with control surfaces.

Experimental Airfoil Design:

The stock NACA 0012 was scaled such that its chord length was 8 units long and it domain was restricted by the x value of ([a/a+2)*8), with "a" ranging from the integers 2-8, inclusive, for each ratio. The connecting spline of the trailing edge was made by finding the 3rd degree polynomial with an order of contact of 1 between the stock NACA 0012 portion and the regression curve portion. The curved regression portion was then graphed with the appropriate domain. In Desmos, the aforementioned functions were graphed in an inequality form such that the inside of the airfoil was shaded. Once the axis and grid were removed (producing a white background), the Desmos graph was exported as a ".png". This ".png" was then converted to a

“.svg” using an online converter. The “.svg” was imported into Fusion 360 and extruded. To maintain the chord length of 12 cm of the control airfoils (as the experimental airfoils are theoretically the stock NACA 0012 airfoil with a smooth bend), the airfoil was appropriately scaled. The average of the lengths of the top and bottom curves of the experimental airfoil was calculated and the scale factor was found by dividing 12 by this average. After the scale, the “press-pull” feature was used to maintain the height of 4 cm.

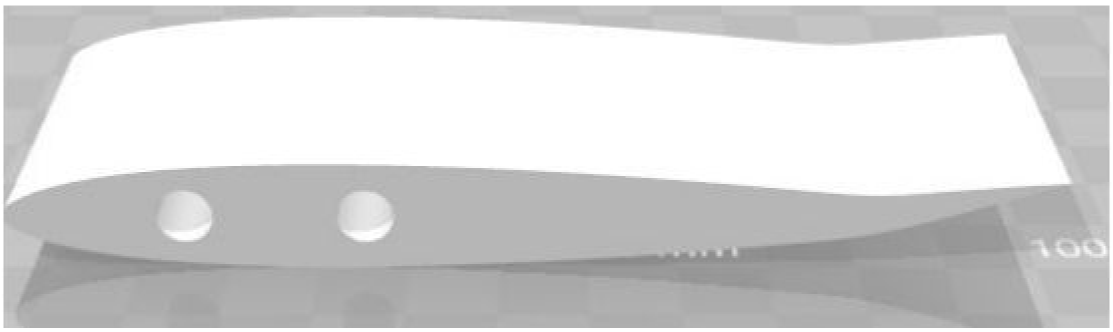

Figure 1.2: Experimental Airfoil with ratio 6:2. Notice how the rigid edge and flexible edge are connected with a smooth transition to mimic that of a morphing wing.

<u>CFD Analysis:</u>

A 70 cm x 13 cm x 14 cm (x/y/z) box was created. This box would mimic the conditions of the wind tunnel possessed by HCI for future standardization purposes should wind tunnel tests be conducted. Boundary Conditions were set. These were:

● Two velocity inputs were tested, one at 13 m/s and one at 20 m/s. This was to simulate the low-speed and high-speed drones.

● The pressure on the trailing edge of the box was set to 0 Pa.

● The sides of the box were set to ‘Slip/Symmetry’, a setting which renders the sides of the box frictionless.

● The material of the imported airfoil was set to ABS (Molded) as this was the only plastic available on the software.

● The material of the box was set to air, as it would simulate the wind tunnel.

● The material of the wing was set to ABS (Molded) as it would simulate a 3D printed airfoil.

Each simulation ran for 260 iterations using these conditions. 260 iterations allowed for CFD to be fully completed as the CFD analysis finished before 260 iterations.

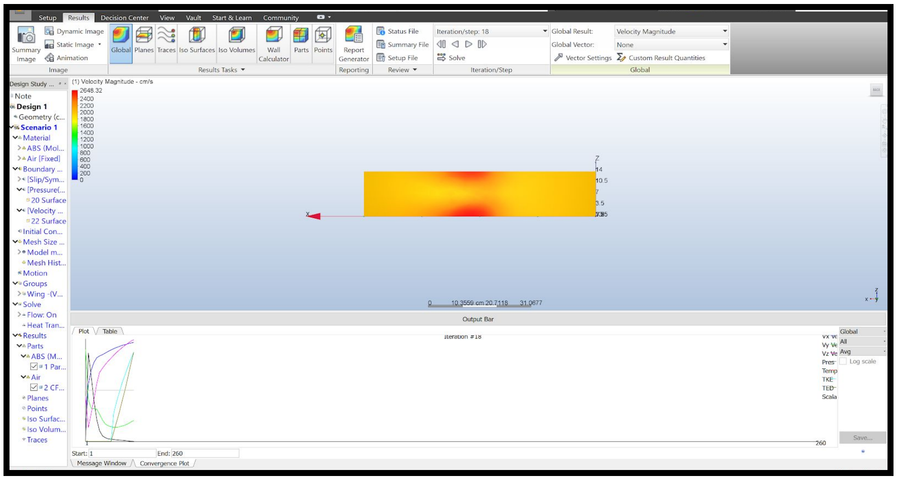

Figure 2.1: Autodesk CFD 2019 going through iterative process. Virtual wind tunnel with pressure variations shown.

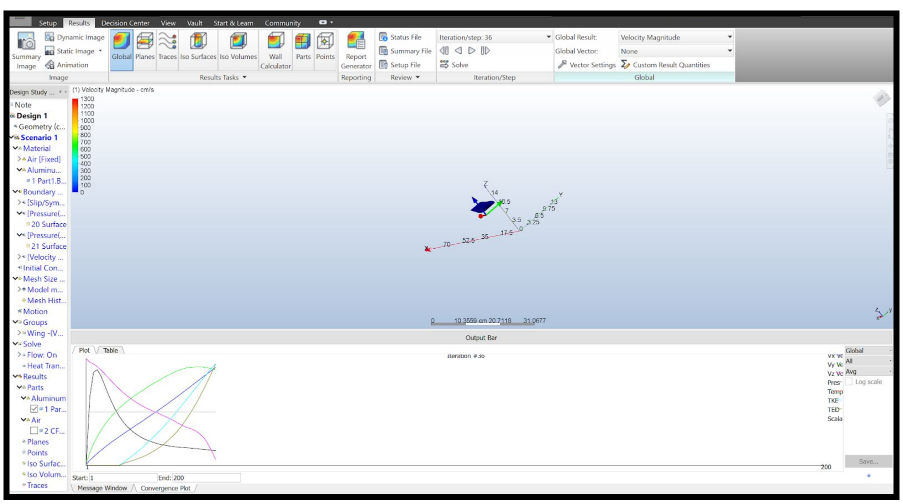

Figure 2.2: Autodesk CFD 2019 going through iterative process. Convergence plot (of pressure, velocity, vectors) is shown. At end-point, graphs will be a straight line, i.e. gradient becomes 0.

D. Results & Discussion

Experimental:

*Figure 3.10: CFD experimental data for **drag** in dyne (20 m/s wind speed)*

	2:2	3:2	4:2	5:2	6:2
Trial 1	6644.60	5476.22	6138.37	6137.29	5860.29
Trial 2	6638.02	5494.78	6151.87	6120.63	5899.24
Trial 3	6638.08	5487.81	6153.44	6142.41	5873.45
Trial 4	6649.69	5489.20	6156.92	6108.69	5883.45
Trial 5	6638.03	5456.99	6154.06	6134.56	5827.68
Average	6641.68	5481.00	6150.93	6128.72	5868.82
SD	5.30	15.02	7.26	13.80	27.05
SE	2.37	6.72	3.245	6.171	12.096

*Figure 3.11: CFD experimental data for **lift** in dyne (20 m/s wind speed)*

	2:2	3:2	4:2	5:2	6:2
Trial 1	12513.80	8907.33	10174.80	9553.36	8783.23
Trial 2	12492.90	9014.91	10244.30	9526.55	8829.43
Trial 3	12492.90	8957.42	10257.70	9468.03	8778.12
Trial 4	12560.40	8949.73	10206.90	9500.89	8803.37
Trial 5	12492.90	8935.40	10257.60	9546.75	8756.57
Average	12510.58	8952.96	10228.26	9519.12	8790.14
SD	29.28	39.56	36.40	35.12	27.56
SE	13.10	17.69	16.28	15.71	12.32

*Figure 3.12: CFD experimental data for **lift:drag** (20 m/s wind speed)*

	2:2	3:2	4:2	5:2	6:2
Trial 1	1.88	1.63	1.66	1.56	1.50
Trial 2	1.88	1.64	1.67	1.56	1.50
Trial 3	1.88	1.63	1.67	1.54	1.49
Trial 4	1.89	1.63	1.66	1.56	1.50
Trial 5	1.88	1.64	1.67	1.56	1.50
Average	1.88	1.63	1.66	1.55	1.50
SD	0.00	0.01	0.00	0.01	0.00
SE	0.00	0.00	0.00	0.00	0.00

*Figure 3.20: CFD experimental data for **drag** in dyne (13 m/s wind speed)*

	2:2	3:2	4:2	5:2	6:2
Trial 1	2934.19	2347.68	2749.88	2696.08	2404.20
Trial 2	2934.63	2337.87	2747.89	2677.44	2403.78
Trial 3	2940.81	2320.22	2749.05	2694.76	2408.91
Trial 4	2940.97	2326.68	2749.20	2691.61	2413.57
Trial 5	2941.06	2390.30	2685.28	2678.94	2406.58
Average	2938.33	2344.55	2736.26	2687.77	2407.41
SD	3.58	27.65	28.51	8.91	4.01
SE	1.60	12.37	12.749	3.983	1.794

*Figure 3.21: CFD experimental data for **lift** in dyne (13 m/s wind speed)*

	2:2	3:2	4:2	5:2	6:2
Trial 1	5350.52	3650.63	4253.87	3697.47	3244.58
Trial 2	5386.85	3593.10	4278.54	3760.37	3250.78
Trial 3	5388.61	3475.93	4253.65	3780.60	3249.90
Trial 4	5387.97	3549.56	4254.25	3735.93	3244.76
Trial 5	5386.36	3590.51	4233.15	3760.66	3245.67
Average	5380.06	3571.95	4254.69	3747.01	3247.14
SD	16.54	64.62	16.08	31.90	2.97
SE	7.40	28.90	7.19	14.27	1.33

*Figure 3.22: CFD experimental data for **lift:drag** in dyne (13 m/s wind speed)*

	2:2	3:2	4:2	5:2	6:2
Trial 1	1.82	1.55	1.55	1.37	1.35
Trial 2	1.84	1.54	1.56	1.40	1.35
Trial 3	1.83	1.50	1.55	1.40	1.35
Trial 4	1.83	1.53	1.55	1.39	1.34
Trial 5	1.83	1.50	1.58	1.40	1.35
Average	1.83	1.52	1.56	1.39	1.35
SD	0.00	0.02	0.01	0.01	0.00
SE	0.00	0.01	0.01	0.01	0.00

*Figure 4.10: CFD control data for **drag** in dyne (20 m/s wind speed)*

	2:2	3:2	4:2	5:2	6:2
Trial 1	7860.56	6459.91	6776.42	6735.65	6598.29
Trial 2	7870.46	6505.74	6862.18	6750.91	6582.14
Trial 3	7863.42	6486.18	6883.34	6803.25	6623.56
Trial 4	7859.58	6471.51	6875.34	6800.14	6600.98
Trial 5	7855.37	6532.95	6799.23	6773.28	6618.29
Average	7861.88	6491.26	6839.30	6772.65	6604.65
SD	5.60	28.92	48.27	29.72	16.62
SE	2.50	12.94	21.59	13.29	7.43

*Figure 4.11: CFD control data for **lift** in dyne (20 m/s wind speed)*

	2:2	3:2	4:2	5:2	6:2
Trial 1	12958.76	9560.67	10503.45	9766.69	9435.56
Trial 2	12925.88	9563.44	10567.76	9788.81	9412.46
Trial 3	12940.67	9534.69	10583.34	9804.56	9467.55
Trial 4	12955.20	9577.83	10576.89	9803.27	9428.73
Trial 5	12943.87	9603.44	10522.78	9791.03	9455.52
Average	4646.51	3438.42	2687.87	2132.17	1709.84
SD	13.03	25.18	35.55	15.25	21.82
SE	5.83	11.26	15.90	6.82	9.76

*Figure 4.12: CFD control data for **lift:drag** in dyne (20 m/s wind speed)*

	2:2	3:2	4:2	5:2	6:2
Trial 1	1.65	1.48	1.55	1.45	1.43
Trial 2	1.64	1.47	1.54	1.45	1.43
Trial 3	1.65	1.47	1.54	1.44	1.43
Trial 4	1.65	1.48	1.54	1.44	1.43
Trial 5	1.65	1.47	1.55	1.45	1.43
Average	1.65	1.47	1.54	1.45	1.43
SD	0.00	0.01	0.01	0.00	0.00
SE	0.00	0.00	0.00	0.00	0.00

Figure 4.20: CFD control data for ***drag*** *in dyne (13 m/s wind speed)*

	2:2	3:2	4:2	5:2	6:2
Trial 1	3626.09	2867.67	3059.06	2997.74	2996.12
Trial 2	3576.82	2870.68	3104.83	3076.16	2977.56
Trial 3	3608.89	2869.47	3087.68	2930.01	2999.03
Trial 4	3638.76	2903.45	3076.51	3080.02	3001.24
Trial 5	3598.97	2907.68	3088.03	3067.49	2987.02
Average	3609.91	2883.79	3083.22	3030.28	2992.19
SD	24.03	19.96	16.87	65.34	9.81
SE	10.75	8.93	7.55	29.22	4.39

Figure 4.21: CFD control data for ***lift*** *in dyne (13 m/s wind speed)*

	2:2	3:2	4:2	5:2	6:2
Trial 1	5765.49	3900.03	4435.56	3987.45	3865.67
Trial 2	5722.34	3903.29	4502.45	3999.24	3822.48
Trial 3	5748.89	3902.14	4476.58	3925.67	3843.45
Trial 4	5769.89	3915.36	4458.90	4001.24	3865.49
Trial 5	5729.83	3918.46	4463.56	4003.27	3843.09
Average	4646.51	3438.42	2687.87	2132.17	1709.84
SD	21.05	8.42	24.56	32.84	18.13
SE	9.41	3.77	10.99	14.69	8.11

Figure 4.22: CFD control data for ***lift:drag*** *in dyne (13 m/s wind speed)*

	2:2	3:2	4:2	5:2	6:2
Trial 1	1.59	1.36	1.45	1.33	1.29
Trial 2	1.60	1.36	1.45	1.30	1.28
Trial 3	1.59	1.36	1.45	1.34	1.28
Trial 4	1.59	1.35	1.45	1.30	1.29
Trial 5	1.59	1.35	1.45	1.31	1.29
Average	1.59	1.36	1.45	1.31	1.29
SD	0.01	0.01	0.00	0.02	0.00
SE	0.00	0.00	0.00	0.01	0.00

Figure 4.30: Lift/Drag ratios for 13m/s. In order of aerodynamic efficiency, it is 2:2, 4:2, 3:2, 5:2, 6:2.

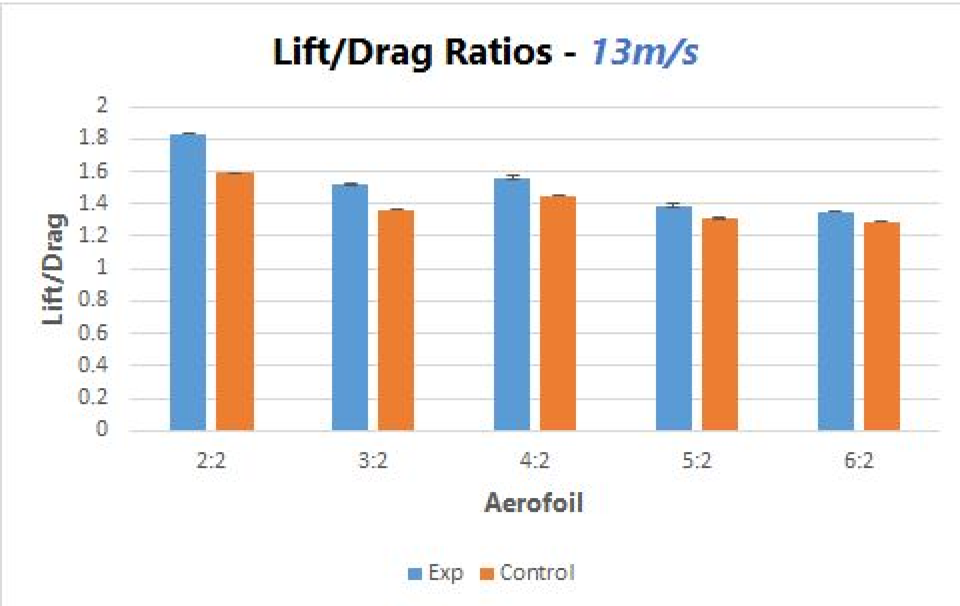

Figure 4.31: Lift/Drag ratios for 20m/s. In order of aerodynamic efficiency, it is 2:2, 4:2, 3:2, 5:2, 6:2.

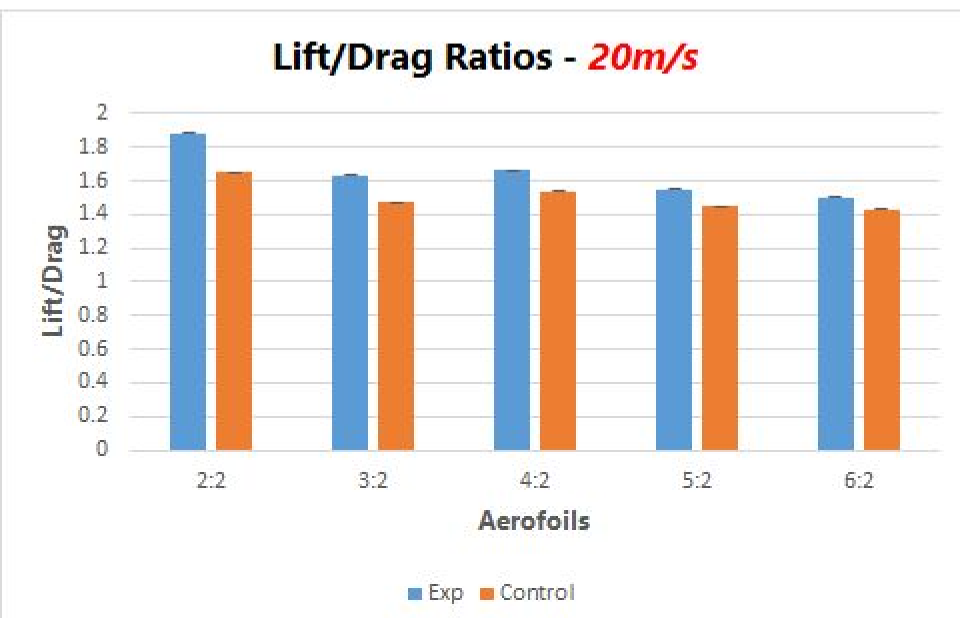

Referencing the above mentioned data, the increase in aerodynamic efficiency provided by the morphing wings is as follows:

20 m/s
Experimental aerofoil on average increased aerodynamic efficiency (lift/drag ratio) by 9.15%.

13 m/s
Experimental aerofoil on average increased aerodynamic efficiency (lift/drag ratio) by 9.05%.

This means that with respect to low-speed and high-speed UAVs, morphing wings potentially increase their aerodynamic efficiency by up to 9.10%.

Takeaways
2:2 was the best ratio as it increased aerodynamic efficiency by an average of 14.5%. This was followed by 3:2 (11.3%), then 4:2 (8.015%), 5:2 (6.85%), and finally 6:2 (4.78%).

Data sets were consistent across 20m/s and 13m/s. It can be seen that experimental aerofoils (morphing wing models) have a significant impact on aerodynamic efficiency.

Discussion
Statistical Analysis: After gathering the data, we ran the Kruskal-Wallis Test to test for the significance of the data. We tested the significance of the results by comparing the data for lift against drag for both experimental and control airfoils at both 20 m/s and 13 m/s speeds. The results were that our *p*-value is 0.00902 for all the tests that we ran, and the result is significant at $p<0.05$.

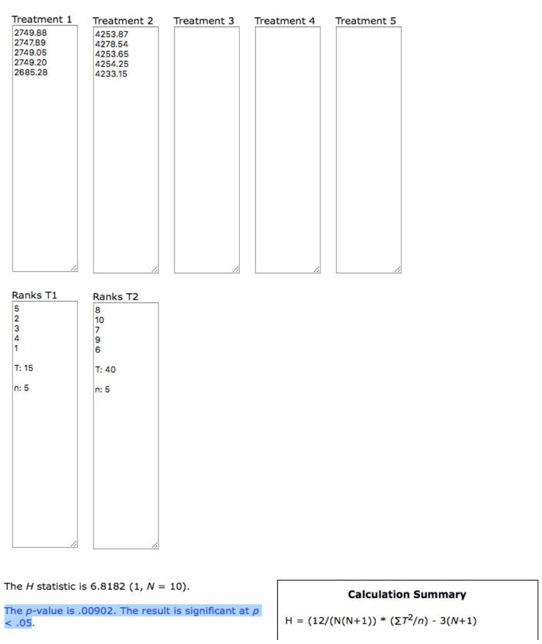

Figure 4.31: example screenshot of the calculation of p-value for lift against drag, experimental 4:2 at 13m/s wind speed.

3:2 may be an anomaly as its lift and drag forces were significantly lower than the others and did not follow their trend, but ultimately the data was consistent over both the experimental and control aerofoils, hence we were confident in continuing in using this
data set.

Referencing the figures above, it can be seen that the lift and drag forces acting on the aerofoils, for both experimental and controls, was greater at 20m/s than 13m/s.

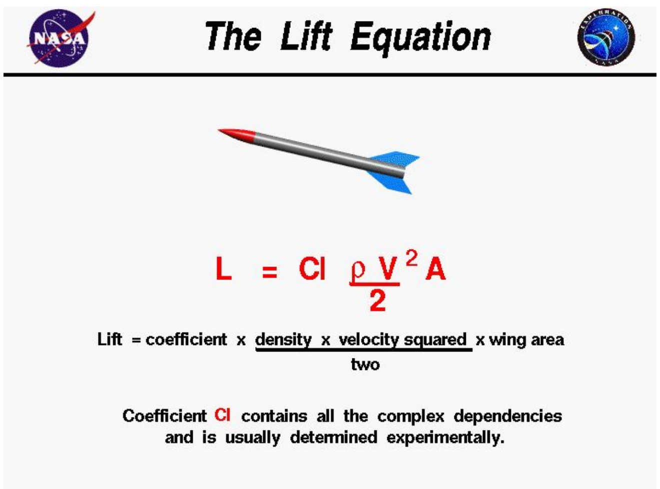

Figure 5.0: Equation for Lift coefficient. As seen, lift, and similarly drag, are directly related to the square of the velocity.

Hence this explains why the increase in the velocity condition from 13m/s to 20m/s results in a sharp increase in the lift and drag forces.

E. Conclusion

It can be concluded that 2:2 is the optimal ratio to increase the aerodynamic efficiency of the aerofoil. There is a relationship between the length of rigid:flexible edge and the aerodynamic efficiency. After 2:2, an increase in the length of the rigid edge with respect to the flexible edge results in a decrease in aerodynamic efficiency.

By integrating this new designs and actuating the morphing wings to the optimal rigid:flexible edge ratios, there will be greener and more efficient travel for UAVs, ultimately making them more favourable by boosting their mobility.

Certain limitations include the lack of realistic testing such as wind tunnel data. In order to mitigate this, the wind tunnel testing can be utilized by Particle Image Velocimetry (PIV). The results from this CFD analysis to build the wind tunnel and test the aerofoils, to obtain more accurate and reliable, realistic results. Furthermore, NACA 0012 was used as it is a commonly tested aerofoil wing. It may not represent the typical aerofoil used in UAVs and hence we can curb this by analysing UAV aerofoils. This was not conducted previously due to the lack of time and resources.

F. References:

- AIN Online. (2017). New Multi-mission Sky Guardian UAS Is More Than A Strike Drone. Retrieved on 15 March, 2018 from https://www.ainonline.com/aviation-news/defense/2017-06-14/new-multi-mission-sky-guardian-uas-more-strike-drone.
- Boldmethod. (2015). How Flaps Work. Retrieved on 15 March, 2018 from http://www.boldmethod.com/learn-to-fly/aircraft-systems/how-flaps-work/.
- Aviation Voice. (2016). FlexSys and Aviation Partners Display Morphing Wing. Retrieved on 15 March, 2018 from https://aviationvoice.com/flexsys-and-aviation-partners-display-morphing-wing-201611070947/.
- The Engineer. (2017). The evolution of the aircraft wing. Retrieved on 30 March, 2018 from https://www.theengineer.co.uk/the-evolution-of-the-aircraft-wing/
- Thyssenkrupp Aerospace. (2018). Aluminium Bar. Retrieved on 31 March from http://www.thyssenkruppaerospace.com/materials/aluminum/aluminum-bar/weight-calculations.html
- Jacobs., Ward., & Pinkerton.. (1932). *The Characteristics of 78 Related Airfoil Sections from Tests in the Variable Density Wind Tunnel*, NACA Report #460. Retrieved on 20 June, 2018 from https://ntrs.nasa.gov/reports/1933/naca-report-460/
- NASA. (2014). The Lift Equation. Retrieved 30 June, 2018 from https://www.grc.nasa.gov/WWW/K-12/rocket/lifteq.html

G. Acknowledgement

We would like to thank our mentor, lab staff Ms Chua, the Academy of Science, Loudoun County Virginia, and Tarun Golla and Adithya Muralilkrishna from AOS. We appreciate all the advice and help given to us on this journey.